AIMS Energy, 6(4): 607–614.
DOI: 10.3934/energy.2018.4.607
Received: 24 July 2018
Accepted: 20 August 2018
Published: 24 August 2018

http://www.aimspress.com/journal/energy

Research article

In-situ investigation of water distribution in polymer electrolyte membrane fuel cells using high-resolution neutron tomography with 6.5 μm pixel size

Saad S. Alrwashdeh[1,*], Falah M. Alsaraireh[1], Mohammad A. Saraireh[1], Henning Markötter[2], Nikolay Kardjilov[2], Merle Klages[3], Joachim Scholta[3] and Ingo Manke[2]

[1] Mechanical Engineering Department, Faculty of Engineering, Mutah University, P.O Box 7, Al-Karak 61710, Jordan
[2] Helmholtz-Zentrum Berlin, Hahn-Meitner-Platz 1, 14109 Berlin, Germany
[3] Zentrum für Sonnenenergie- und Wasserstoff-Forschung Baden Württemberg (ZSW), Helmholtzstraße 8, 89081 Ulm, Germany

* **Correspondence:** Email: saad_r1988@yahoo.com; Tel: +962796430481.

Abstract: In this feasibility study, high-resolution neutron tomography is used to investigate the water distribution in polymer electrolyte membrane fuel cells (PEMFCs). Two PEMFCs were built up with two different gas diffusion layers (GDLs) namely Sigracet® SGL-25BC and Freudenberg H14C10, respectively. High-resolution neutron tomography has the ability to display the water distribution in the flow field channels and the GDLs, with very high accuracy. Here, we found that the water distribution in the cell equipped with the Freudenberg H14C10 material was much more homogenous compared to the cell with the SGL-25BC material.

Keywords: polymer electrolyte membrane fuel cell; water transport; high resolution neutron tomography; gas diffusion layers

1. Introduction

The Fuel cell technology plays a major role in offering a pollution free alternative energy supply in contrast to burning fossil fuels [1–6]. Fuel cells are an applicable technology for mobile and

stationary applications. A common example of mobile systems is the automotive sector, where polymer electrolyte membrane fuel cells (PEMFC) are considered the most favorable fuel cell type due to their high output power density and flexible operating conditions [7,8]. They are also suitable to provide combined heat and electric power in stationary energy systems to maximize efficiency [9,10].

Especially under critical operating conditions where accumulated product water causes flooding an optimization of the water transport in the PEMFC leads to an improved efficiency. Such conditions include temperatures below 60 ℃ as well as high current densities that both lead to increased water agglomerations [11–13].

There are many different materials used in PEMFCs, which affect the water transport in the cells. Through the material properties the interaction with liquid water during operation influences the cell performance. Optimization of the water transport in the fuel cell layers leads to enhance the efficiency especially under critical operation conditions that promote flooding. Such as temperatures below 60 ℃ as well as high currents. A more detailed understanding of the influence of material types was obtained by analyzing several materials [14–17]. So far, X-Ray based imaging methods have been applied to study the liquid water evolution and distribution also during cell operation [18–26].

Neutron imaging can be used as complementary method for fuel cell research because neutrons are strongly affected by hydrogen, imaging methods based on neutrons are very helpful to study hydrogen distributions within the cell materials [23–27]. For the same reason, neutron imaging is used to study the water distribution in operating fuel cells [14, 28–33].

In this study, High-resolution neutron tomography has been used for the investigation of the water distribution in PEMFCs. The detector system was set to a pixel size of ~6.5 μm, which is enough to resolve even smaller water droplets in the GDL of the cells in sufficient detail. Even the catalyst can be observed, which is hardly possible with X-Rays due to the high absorbing platinum [11].

2. Method and experiments

The neutron imaging beam line CONRAD II (COld Neutron Radiography) is used in order to investigate material structure as well as dynamic processes of the water transport in the cell [27–30]. It allows to create radiographs using cold neutrons, which are product of the 10 MW research reactor BER II and moderated in a cold neutron source containing liquid hydrogen. Subsequently they are transported through a neutron guide to the experiment. The neutron beam at CONRAD is polychromatic mainly with wavelengths between 2 and 6 Å and a maximum intensity at about 3.0 Å. The tomography measurements of the fuel cells discussed here are performed 5 m from the end of the neutron guide as shown in Figure 1 [31].

Behind the sample as close as possible a detector system consisting of a scintillator, mirror, lens and CCD camera is placed [31–33]. When neutrons, which are transmitted and scattered by the sample, hit the scintillator, photons in the visible spectrum are emitted. The scintillator used for the tomography measurements is a gadox screen (Gd_2O_2S(Tb) with 20 μm thickness.

The photons are projected onto the camera by a mirror/lens combination. The used Andor DW436 camera contains a 16 bit chip with (2048 × 2048) pixels, each corresponding to a size of 6.5 μm. The CCD sensor is continuously cooled to –50 ℃ to ensure thermal noise being as low as

possible. With the used optics an imaging field of view of (13 × 13) mm ²is chosen. Each projection is acquired with an exposure time of 15 s then the projections collected for each tomographic scan.

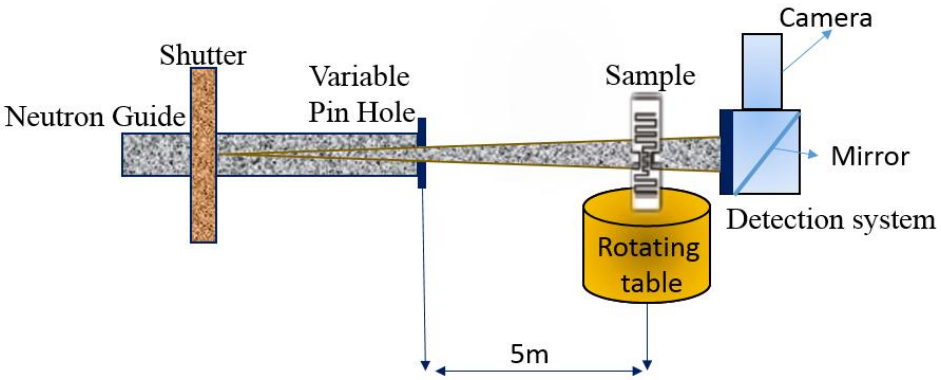

Figure 1. Schematic drawing of the imaging setup at the CONRAD instrument.

2.1 Fuel cell setup

In both cells the regulation of the cell temperature is carried out by using a cooling circuit with deuterium oxide (D_2O). Compared to hydrogen, the attenuation coefficient of deuterium is much smaller [34–36]. As a result, D_2O hardly attenuates the neutron beam and can only be seen faintly in radiographs and tomography. The flow field of the cooling circuit is embedded in the backside of the bipolar plates and is connected with a secondary water coolant circuit via a heat exchanger to maintain a stable temperature distribution.

The two tomography cells have an active area of 5.4 cm ². One contains Sigracet® SGL 25BC GDLs and the other Freudenberg H14C10 GDLs.

Each cell is equipped with three flow field channels on anode and cathode side, respectively. 0.5 mm wide meander-shaped channels are milled into the graphite composite material, through which the supply gases, hydrogen on the anode and air on the cathode side, flow from top to bottom. More details of the fuel cell design can be found in previous works [37]. The presented measurements are conducted at a current density of 1 A.cm^{-2}and a cell temperature of 65 ℃, while the cell is supplied with gases of 120% relative humidity. Via gas flow controllers λ, the ratio of the supplied and consumed gases, is set to 5 for anode (H_2) as well as cathode (air) side.

3. Results

Figure 2A–C shows tomographic slices of the fuel cell equipped with Sigracet® SGL-25BC material and Figure 2D–F the cell with Freudenberg-H14C10 material. These are parallel to the active layer and positioned in the anode flow field (A and D), in the membrane electrode assembly MEA (B and E) and in the cathode flow field (C and F). It can be seen in the images of the cell with Sigracet® SGL-25BC material that the water accumulates in the corner of the anode channel turnings (see Figure 2A), while it blocks one channel on cathode side with a big droplet due to the high condensation because of the material type. In the MEA, basically in the two gas diffusion layers, water is appearing as small droplets, which are marked in figure 2B with white arrows. The water in the cell with the Freudenberg H14C10 material is distributed all over the cell channels in smaller

droplets which aid in a homogeneous distribution of the water inside the cell and enhance the membrane humidity level (Figure 2D) while it is focused on the corners and edges of the cathode channels which will block the channel and reduce the level of the gases supply for a sufficient reaction finally that will aid in a reduction in the cell performance (Figure 2F). The water in Freudenbergs H14C10 appears more in big droplets compared to the Sigracet® SGL-25BC material as in the Figure 2E White arrows. Please note that by using tomography, there is the ability to observe the water in the gas diffusion layers separately from the channels, which is not possible by using radiography.

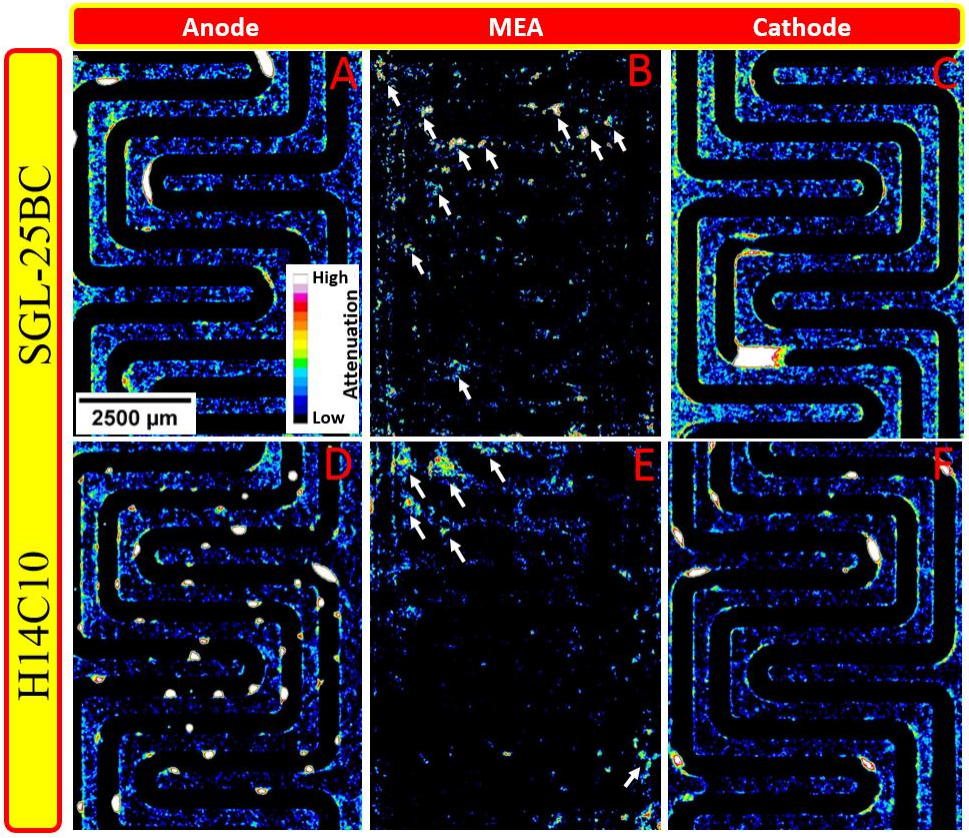

Figure 2. Tomographic slices through the fuel cells with Sigracet® SGL-25BC and Freudenberg H14C10 GDL materials at the position of the anode (A, D), the MEA (B, E) and the Cathode (C, F).

The graphs in Figure 3 show the water volume in both cells. It can be noted that the water volume contained in the Sigracet® SGL 25BC material is less compared to the cell with Freudenberg H1410 material, especially in the region of the MEA. The water in the Freudenberg H1410 material distributed all over the cell in the anode and cathode sides comparing to the water distribution in Sigracet® SGL 25BC material also more water can be found in the MEA region of Freudenberg H1410 material which can play a major role in humidify the membrane and enhance the cell performance comparing to cell containing the Sigracet® SGL 25BC material. Note that the water blocked a complete channel in the cathode side of the cell containing Sigracet® SGL 25BC also concentrated in the corner of the channels.

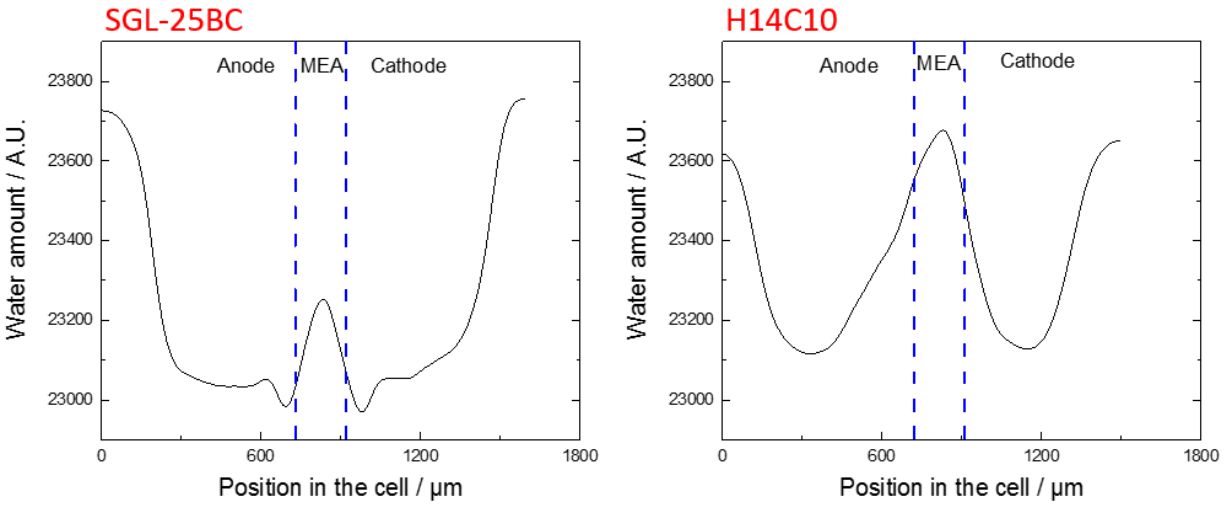

Figure 3. water volume of the fuel cells with Sigracet® SGL 25BC and Freudenberg H1410.

4. Discussion

Despite the same operating parameters more water was found in the MEA of the cell containing the Freudenberg H14C10 material than in the MEA of the cell with Sigracet® SGL 25BC material (see Figure 3). This water is also more homogenously distributed. No larger water agglomerations were found that may yield as bottle necks either affecting the gas stream (e.g., flooding). As there were no bigger areas found without any water, which might affect the membrane humidification (dehydration). In contrast, in the MEA of the cell with Sigracet® SGL 25BC less water is found. It can be assumed that this may reduce humidification of the membrane in the top area and cause a dehydration effect. On the other hand, the larger overall water amount in the MEA of the cell containing Freudenberg H1410 material can also improve membrane humidity and thus ion conductivity at most locations in the cell.

5. Conclusions

Liquid water inside two cells with a specially adapted PEMFC design with a three-channel flow field system containing two different GDLs were studied. High resolution neutron tomography has the ability to detect the water in the MEA even inside the catalyst of the PEMFCs. The technique is a powerful tool to detect liquid water inside the components of PEMFCs. The following points can be concluded in this study:

(1) The spatially resolved water distribution in the flow fields, GDLs and MEA can be detected and studied using high-resolution neutron tomography.

(2) In the presented example we found an overall higher amount of liquid water in the cell containing Freudenbergs H14C10 GDL compared to SGLs 25BC GDL material.

This study provides insights in to the distribution of liquid water in complete operated fuel cells and is not hindered at the catalyst layer, which is still an obstacle when using X-Ray CT. High resolution neutron tomography may contribute to future simulation studies about the water distribution and transport processes in MEAs [38].

Conflict of interest

All authors declare no conflicts of interest in this paper.

References

1. Hoogers G (2003) Fuel Cell Technology Handbook. Boca Raton, FL: CRC Press LLC.
2. Vielstich W, Lamm A, Gasteiger HA (2003) Handbook of fuel cells–fundamentals, technology and applications. Chichester: John Wiley & Sons.
3. Alrwashdeh SS, Manke I, Markötter H, et al. (2017) In operando quantification of three-dimensional water distribution in nanoporous carbon-based layers in polymer electrolyte membrane fuel cells. *ACS Nano* 11: 5944–5949.
4. Alrwashdeh SS, Manke I, Markötter H, et al. (2017) Neutron radiographic in operando investigation of water transport in polymer electrolyte membrane fuel cells with channel barriers. *Energ Convers Manage* 148: 604–610.
5. Alrwashdeh SS, Manke I, Markötter H, et al. (2017) Improved performance of polymer electrolyte membrane fuel cells with modified microporous layer structures. *Energy Technol* 5: 1612–1618.
6. Saad SA, Henning M, Haußmann J, et al. (2017) Investigation of water transport in newly developed micro porous layers for polymer electrolyte membrane fuel cells. *Appl Microscopy* 47: 101–104.
7. Mehta V, Cooper JS (2003) Review and analysis of PEM fuel cell design and manufacturing. *J Power Sources* 114: 32–53.
8. Carrette L, Friedrich KA, Stimming U (2000) Fuel cells: principles, types, fuels, and applications: WILEY-VCH Verlag GmbH, Weinheim.
9. Barelli L, Bidini G, Gallorini F, et al. (2012) Dynamic analysis of PEMFC-based CHP systems for domestic application. *Appl Energ* 91: 13–28.
10. Gigliucci G, Petruzzi L, Cerelli E, et al. (2004) Demonstration of a residential CHP system based on PEM fuel cells. *J Power Sources* 131: 62–68.
11. Krüger P, Markötter H, Haußmann J, et al. (2011) Synchrotron X-ray tomography for investigations of water distribution in polymer electrolyte membrane fuel cells. *J Power Sources* 196: 5250–5255.
12. Manke I, Hartnig C, Kardjilov N, et al. (2009) In-situ investigation of the water distribution in PEM fuel cells by neutron radiography and tomography. *Mater Test* 51: 219–226.
13. Alrwashdeh SS, Markötter H, Haußmann J, et al. (2016) Investigation of water transport dynamics in polymer electrolyte membrane fuel cells based on high porous micro porous layers. *Energy* 102: 161–165.
14. Cindrella L, Kannan AM (2009) Membrane electrode assembly with doped polyaniline interlayer for proton exchange membrane fuel cells under low relative humidity conditions. *J Power Sources* 193: 447–453.
15. Cindrella L, Kannan AM, Ahmad R, et al. (2009) Surface modification of gas diffusion layers by inorganic nanomaterials for performance enhancement of proton exchange membrane fuel cells at low RH conditions. *Int J Hydrogen Energ* 34: 6377–6383.

16. Mohanraju K, Sreejith V, Ananth R, et al. (2015) Enhanced electrocatalytic activity of PANI and CoFe2O4/PANI composite supported on graphene for fuel cell applications. *J Power Sources* 284: 383–391.
17. Cindrella L, Kannan AM, Lin JF, et al. (2009) Gas diffusion layer for proton exchange membrane fuel cells—A review. *J Power Sources* 194: 146–160.
18. Chevalier S, Ge N, George MG, et al. (2017) Synchrotron X-ray radiography as a highly precise and accurate method for measuring the spatial distribution of liquid water in operating polymer electrolyte membrane fuel cells. *J Electrochem Soc* 164: F107–F114.
19. Ge N, Chevalier S, Lee J, et al. (2017) Non-isothermal two-phase transport in a polymer electrolyte membrane fuel cell with crack-free microporous layers. *Int J Heat Mass Transfer* 107: 418–431.
20. Antonacci P, Chevalier S, Lee J, et al. (2015) Feasibility of combining electrochemical impedance spectroscopy and synchrotron X-ray radiography for determining the influence of liquid water on polymer electrolyte membrane fuel cell performance. *Int J Hydrogen Energ* 40: 16494–1502.
21. Lee J, Hinebaugh J, Bazylak A (2013) Synchrotron X-ray radiographic investigations of liquid water transport behavior in a PEMFC with MPL-coated GDLs. *J Power Sources* 227: 123–130.
22. Arlt T, Grothausmann R, Manke I, et al. (2013) Tomographic methods for fuel cell research. *Mater Test* 55: 207–213.
23. Eberhardt SH, Marone F, Stampanoni M, et al. (2016) Operando X-ray tomographic microscopy imaging of HT-PEFC: A comparative study of phosphoric acid electrolyte migration. *J Electrochem Soc* 163: F842–F847.
24. Arlt T, Klages M, Messerschmidt M, et al. (2017) Influence of artificially aged gas diffusion layers on the water management of polymer electrolyte membrane fuel cells analyzed with in-operando synchrotron imaging. *Energy* 118: 502–511.
25. Chevalier S, Ge N, Lee J, et al. (2017) Novel electrospun gas diffusion layers for polymer electrolyte membrane fuel cells: Part II. In operando synchrotron imaging for microscale liquid water transport characterization. *J Power Sources* 352: 281–290.
26. Matsui H, Ishiguro N, Uruga T, et al. (2017) Operando 3D visualization of migration and degradation of a platinum cathode catalyst in a polymer electrolyte fuel cell. *Angew Chem Int Ed Engl* 56: 9371–9375.
27. Kardjilov N, Hilger A, Manke I, et al. (2011) Neutron tomography instrument CONRAD at HZB. *Nucl Instrum Meth A* 651: 47–52.
28. Kardjilov N, Manke I, Hilger A, et al. (2011) Neutron imaging in materials science. *Mater Today* 14: 248–256.
29. Kardjilov N, Hilger A, Manke I, et al. (2015) Imaging with cold neutrons at the CONRAD-2 Facility. In: Lehmann EH, Kaestner AP, Mannes D, editors, Proceedings of the 10th World Conference on Neutron Radiography. Amsterdam: *Elsevier Science Bv*, 60–66.
30. Kardjilov N, Hilger A, Manke I, et al. (2016) CONRAD-2: the new neutron imaging instrument at the Helmholtz-Zentrum Berlin. *J Appl Crystallogr* 49: 195–202.
31. Williams SH, Hilger A, Kardjilov N, et al. (2012) Detection system for microimaging with neutrons. *J Instrum* 7: 1–25.
32. Kardjilov N, Dawson M, Hilger A, et al. (2011) A highly adaptive detector system for high resolution neutron imaging. *Nucl Instrum Meth A* 651: 95–99.

33. Totzke C, Manke I, Hilger A, et al. (2011) Large area high resolution neutron imaging detector for fuel cell research. *J Power Sources* 196: 4631–4637.
34. Banhart J (2008) Advanced tomographic methods in materials research and engineering. Oxford, UK: Oxford University, Press.
35. Manke I, Hartnig C, Kardjilov N, et al. (2008) Characterization of water exchange and two-phase flow in porous gas diffusion materials by hydrogen-deuterium contrast neutron radiography. *Appl Phys Lett* 92: 337–347.
36. Cho KT, Mench MM (2012) Investigation of the role of the micro-porous layer in polymer electrolyte fuel cells with hydrogen deuterium contrast neutron radiography. *Phys Chem Chem Phys* 14: 4296–4302.
37. Haussmann J, Markotter H, Alink R, et al. (2013) Synchrotron radiography and tomography of water transport in perforated gas diffusion media. *J Power Sources* 239: 611–622.
38. Weber AZ, Borup RL, Darling RM, et al. (2014) A critical review of modeling transport phenomena in polymer-electrolyte fuel cells. *J Electrochem Soc* 161: F1254–F1299.